Structural Engineering and Mechanics, *Vol. 64, No. 2 (2017) 155-171*
DOI: https://doi.org/10.12989/sem.2017.64.2.155

Experimental and FE simulations of ferrocement columns incorporating composite materials

Yousry B.I. Shaheen[1a], Ashraf M. Mahmoud[*2] and Hala M. Refat[3b]

[1]*Civil Engineering Department, Faculty of Engineering, Menoufia University, Menoufia, Egypt*
[2]*Civil Engineering Department, Faculty of Engineering, Modern University for Technology and Information (MTI), Al-Mokattam, Cairo, Egypt*
[3]*Civil Engineering Department, Faculty of Engineering, Benha University, Benha, Egypt*

(Received January 19, 2017, Revised June 2, 2017, Accepted June 5, 2017)

Abstract. This paper presents a proposed method for producing reinforced composite concrete columns reinforced with various types of metallic and non metallic mesh reinforcement. The experimental program includes casting and testing of twelve square columns having the dimensions of 100 mm×100 mm×1000 mm under concentric compression loadings. The test samples comprise all designation specimens to make comparative study between conventionally reinforced concrete column and concrete columns reinforced with welded steel mesh, expanded steel mesh, fiber glass mesh and tensar mesh. The main variables are the type of innovative reinforcing materials, metallic or non metallic, the number of layers and volume fraction of reinforcement. The main objective is to evaluate the effectiveness of employing the new innovative materials in reinforcing the composite concrete columns. The results of an experimental investigation to examine the effectiveness of these produced columns are reported and discussed including strength, deformation, cracking, and ductility properties. Non-linear finite element analysis; (NLFEA) was carried out to simulate the behavior of the reinforced concrete composite columns. The numerical model could agree the behavior level of the test results. ANSYS-10.0 Software. Also, parametric study is presented to look at the variables that can mainly affect the mechanical behaviors of the model such as the change of column dimensions. The results proved that new reinforced concrete columns can be developed with high strength, crack resistance, and high ductility properties using the innovative composite materials.

Keywords: ferrocement; concrete columns; composite material; experimental; FE modeling; strength; parametric study

1. Introduction

Ferrocement can be defined as a thin wall reinforced concrete commonly constructed of hydraulic cement mortar reinforced with closely spaced layers of continuous and relatively small diameter wire mesh. Ferrocement is ideally suited for structures in which predominant membrane stresses occur. As a result, it has been extensively used to construct different element such as, tanks, roofs, bridge decks…etc.

For reinforced concrete structures, the column is the most important and critical element that can determine the behavior and failure mode of the structure. In the last few decades, incidence of failures of reinforced concrete structures has been seen widely because of increasing service loads, seismic loads and/or durability problems. Mansur and Paramasivam (1990) carried out an experimental investigation on ferrocement box-section short columns with and without concrete infill under axial and eccentric compression.

∗Corresponding author, Associate Professor
E-mail: ashraf_amin78@yahoo.com
[a]Professor
E-mail: Ybishaheen@yahoo.com
[b]Lecturer
E-mail: hala.abusafa@bhit.bu.edu.eg

The studied parameters were the types, arrangements, and volume fraction of reinforcement. Test results indicated that a ferrocement box- section can be used as a structural columns. Welded wire mesh has been found to perform better than an equivalent amount of woven mesh. Another interesting research was done by Ahmed *et al*. (1994). The possibility of using ferrocement as a retrofit material for masonry columns is investigated.

Uniaxial compression tests were performed on three uncoated brick columns, six coated brick columns with 25 mm plaster and another six columns coated with 25 mm thick layer of ferrocement. The study demonstrated that the use ferrocement coating strengthens brick columns significantly and improves their cracking resistance. Kaushik *et al*. (1994) carried out an investigation for ferrocement encased concrete columns. They have investigated short circular as well as square columns with unreinforced and reinforced cores. It was seen that the ferrocement encasement increases the strength and ductility of the columns for both axial and eccentric loading conditions. Nedwell *et al*. (1994) conducted a preliminary investigation into the repair of short square columns using ferro-cement. Also, several investigations have been reported on different ferrocement elements under axial load and eccentric compression (Fahmy *et al* 1999, 1999, 2004, 2004, 2005). Abdel-Tawab (2006) investigated the use of U-shaped ferrocement permanent forms for the construction of beams. Hazem (2009) used non-metallic reinforcement for

ISSN: 1225-4568 (Print), 1598-6217 (Online)

the U-shaped ferrocement forms instead of the conventional steel mesh. Applying the ferrocement concept in construction of concrete beams incorporating reinforced mortar permanent forms is investigated by Fahmy *et al*. (2013). This paper presented the results of an investigation aimed at developing reinforced concrete beams consisting of pre-cast permanent Ushaped reinforced mortar forms filled with different types of core materials to be used as a viable alternative to the conventional reinforced concrete beam. Singh *et al.* (2015) studied the effect of the strength of ferrocement jackets for initially damaged exterior RC beam-column joints by loading these specimens up to failure. The improvement in ultimate and yield load carrying capacity with increase in stiffness of the ferrocement jacketed joints in comparison to control joint was discussed. Sirimontree *et al.* (2015) focused on behaviors of reinforced concrete (RC) column encased by longitudinal steel and ferrocement under static axially loading. Significant improvement of strength and ductility of strengthened column over reference column without strengthening is observed. El-Kholy and Dahish (2015) presented investigation for using single Expanded Metal Mesh (EMM) layer combined, in practical configuration, with various volumetric ratios of ties as lateral reinforcement for square short RC columns. Significant improvement in the strength and ductility for columns confined with proposed lateral reinforcement is observed. Also, high reduction in ties volumetric ratio with no loss in ultimate load could be achieved by installing the EMM layer. Onathara and Martin (2015) presented an experimental simulation carried out on the RC columns strengthened using ferrocement and steel angles, in order to investigate the effectiveness of these strengthening methods on the column behavior such as load-carrying capacity, deflection and ductility. Kaish *et al.* (2016) presented efficient techniques to overcome the drawbacks of conventional square ferrocement jackets (CSFJ) in strengthening of short square-shaped RC columns. The experimental investigation of selected variations among the proposed techniques, such as strengthening all column corners or reducing the concentration of stresses at corners, confirmed that these techniques were very efficient in improving the CSFJ technique in terms of load carrying and deformation capacities. Kumar and Patel (2016) carried out a numerical investigation on axially loaded concrete columns strengthened with stainless steel wire mesh (SSWM) as an alternative material for strengthening of structural elements similar to fiber reinforced polymer (FRP). The studied parameters were concrete grade, heights of columns, and number of SSWM wraps. Numerical results indicated that an increase in axial capacity is observed with different number of SSWM wraps. Kwon *et al.* (2016) investigated experimentally the effect of using Velcro materials to improve the seismic performance of columns in RC frame structures. The studied variables are the strength, displacement, failure mode, ductility capacity and amount of dissipated energy of the studied RC-columns. It was concluded that the strengthening method using Velcro could be used to enhance the seismic behavior of RC-columns. Shaheen *et al.* (2016) carried out experimental and FE investigation on ribbed ferrocement plates. The effect of using the ferrocement materials such as expanded metal mesh and woven steel mesh, in enhancing the strength, ductility ratio and energy absorption properties of the ribbed plates were studied compared to the conventional RC ribbed plates.

The main objective of this study is to produce elements acting as columns bearing elements using the unique properties of ferrocement concept. These developed elements can replace the conventional reinforced concrete elements because they are more economical and lighter in weight. Also, the study aimed at decreasing the cost of production of the new elements by using cheap materials like light weight, durable reinforcing materials such as polypropylene fibers, polyethylene mesh, fiber glass mesh, tensar mesh, expanded steel mesh and galvanized steel meshes. Twelve reinforced concrete columns with different volume fraction of steel reinforcement and different number of metallic and non metallic mesh reinforcement layers were tested up to failure. In addition, the current research aims to simulate the tested ferrocement columns by finite element ANSYS 10 program to investigate their mechanical behavior up to failure.

2. Experimental program

Columns test specimens were classified into twelve designations depending on the type of reinforcing materials used. All designations having the dimensions of 100×100 mm in cross section and 1000 mm long were reinforced with new composite materials. Table 1 shows the details of all designation specimens. The specific surface area is a property of specimen defined as the total surface area per unit of bulk volume, with units of cm^2/cm^3. Fig. 1 shows the reinforcement arrangements for all the twelve designations columns. Different materials were used to produce the specimens including, mortar, steel meshes, and polypropylene fibers. Coarse aggregate was not used in the mortar to produce flow able mortar that can be cast easily into the molds without causing honeycombing. Super plasticizer was used to provide high workability to ease the process of casting. Different types of meshes metallic and non metallic were used. Various types of reinforcing materials were employed as shown in Fig. 2. The longitudinal volume fraction is defined according to the Ferrocement Model Code (2001) as follows

$$V_{rL} = \frac{Nn\pi d_w^{\ 2}}{4tB} \quad (1)$$

[For welded and woven wire mesh]

$$V_{rL} = .65\frac{NW_r}{t\gamma_r} \quad (2)$$

[For expanded wire mesh]

Where:

B = width of the specimen
d_w = diameter of mesh wire
N = number of layers of mesh
n = number of bars in one layer in the cross section
t = thickness of ferrocement layer for calculating the

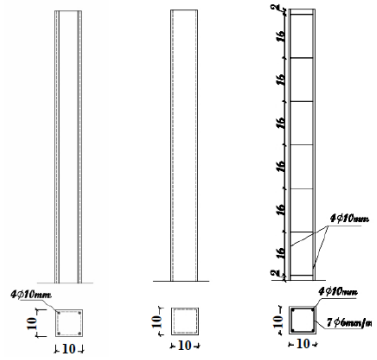

(a) Reinforcement arrangements for columns C1, C2, and C3

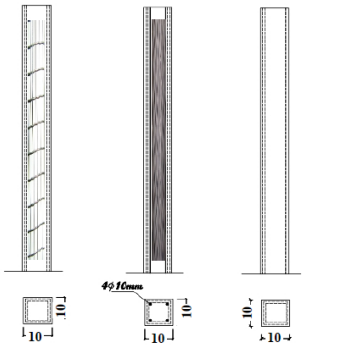

(b) Reinforcement arrangements for columns C4, C5, and C6

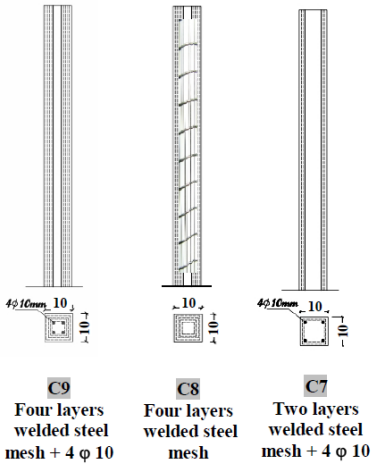

(c) Reinforcement arrangements for columns C7, C8, and C9

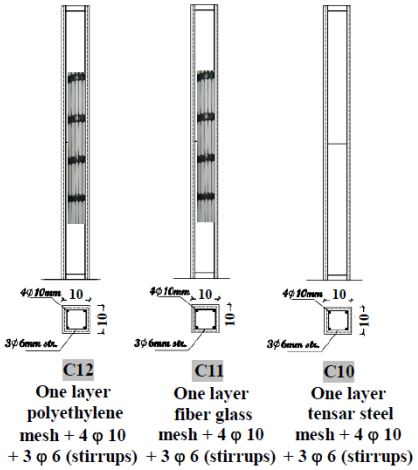

(d) Reinforcement arrangements for columns C10, C11, and C12

Fig. 1 Reinforcement arrangements for the designation

Table 1 Details of the designation specimens

Designation	No. of layers	Reinforcement details (Metallic or non metallic)	Volume fraction % (V_{rL})	Specific surface area, cm^{-1}
C1 (Control)	-------	4 Φ 10 mm+7Φ 6 / m (stirrups)	3.8560	0.1731
C2	one	one layer expanded steel mesh	0.7337	0.1467
C3	one	one layer expanded steel mesh + 4 Φ 10 mm	3.8776	0.2450
C4	two	two layers expanded mesh	1.4674	0.2934
C5	two	two layers expanded steel mesh + 4 Φ 10 mm	4.6113	0.3920
C6	two	two layers welded steel mesh	0.5350	0.0275
C7	two	two layers welded steel mesh + 4 Φ 10 mm	3.6789	0.1530
C8	four	four layers welded steel mesh	1.0700	0.0550
C9	four	four layers welded steel mesh + 4 Φ 10 mm	4.2139	0.1806
C10	one	one layer tensar mesh + 4 Φ 10 mm + 3Φ 6 mm / m (stirrups)	4.2019	0.1990
C11	one	one layer fiber glass mesh+ 4 Φ10 mm + 3Φ6 mm / m (stirrups)	3.7920	0.1386
C12	one	one layer polyethylene mesh + 4Φ10 mm + 3Φ6 mm (stirrups)	5.4720	0.4280

volume fraction in the layer
= thickness of the web for calculating the volume fraction in the web
W_r = unit weight of reinforcing mesh
γ_r = density of reinforcing material

All produced test designations were tested under axial compression loadings until failure. Designation C1 consisted of casting and testing a conventional concrete

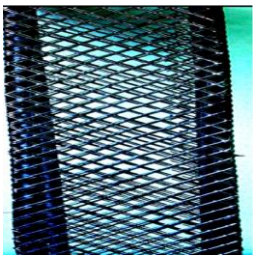
(a) Expanded steel

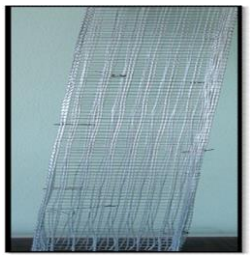
(b) Welded steel


(c) Tensar

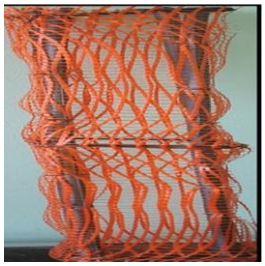
(d) Fiber glass


(e) Polyethelen mesh

Fig. 2 Configurations of composites materials

column. Designation C2 comprised casting and testing column which was reinforced with one layer of expanded steel mesh only. Designation C3 is the same as designation C2, incorporating four skeletal steel bars in the longitudinal direction. Designation C4 comprised casting and testing column, which was reinforced with two layers of expanded steel mesh only. Designation C5 is the same as designation C4, incorporating four skeletal steel bars in the longitudinal direction. Designation C6 comprised casting and testing column, which was reinforced with two layers of welded steel mesh only. Designation C7 is the same as designation C6, incorporating four skeletal steel bars in the longitudinal direction. Designation C8 comprised casting and testing column, which was reinforced with four layers of welded steel mesh only. Designation C9 is the same as designation C8, incorporating four skeletal steel bars in the longitudinal direction. Designation C10 comprised casting and testing column, which was reinforced with one layer of tensar mesh, incorporating four skeletal steel bars in the longitudinal direction and stirrups.

Designation C11 comprised casting and testing column, which was reinforced with one layer of fiber glass mesh, incorporating four skeletal steel bars in the longitudinal direction and stirrups. Finally, designation C12 comprised casting and testing column that was reinforced with one layer of polyethylene glass mesh, incorporating four skeletal steel bars in the longitudinal direction and stirrups. The main variables studied were the number of reinforcing mesh layers, type of mesh used, volume fraction of

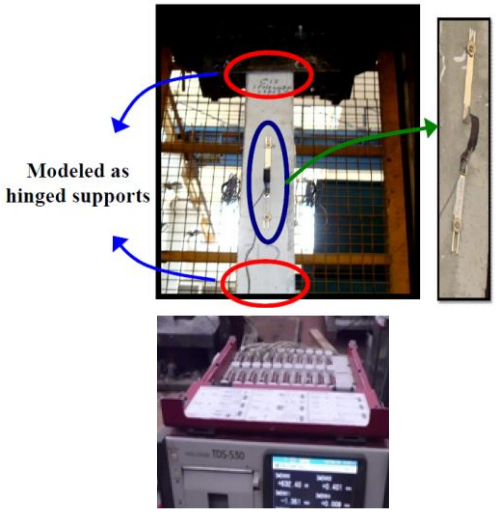

Fig. 3 Test setup and data logger used in recording results

reinforcing steel and combination of mesh and skeletal steel bars. All test specimens were supplied with four displacement transducers (type P1) of gauge length 200 mm and was placed on four sides of the test specimen to measure the vertical displacement versus load during the test. In addition, two linear variable differential transducers (LVDT) were placed at the center of two opposite sides of the test specimen to measure the horizontal displacement.

All test specimens were tested under concentric loadings at the column ends until failure. The main components of the testing facility are: Control Station, Loading Cells and Testing Frame. The load was applied via loading cell which was acting at the column head. The load was incrementally applied with an increment of 5.0 to 20 kN for all the test specimens as shown in Fig. 3. All the deformation characteristics, cracking patterns and strengths were extensively measured at all stages of loadings.

2.1 Materials properties

2.1.1 Cement

Ordinary Portland cement was used throughout this work (O.P.C) with a specific surface area (Blaine fineness) of 3050 cm^2/gm. Typical compounds of the cement was as follows: C_3S=65.1 percent, C_2S=7.6 percent, C_3A=10.8 percent and C_4AF=7.3 percent. The alkali content (as Na_2O equivalent) was 0.29 mass percent.

2.1.2 Silica fume

Silica fume (S.F.) was employed in the present work to enhance the strength of ferrocement mortar and/or concrete core. Based on Abdel Naby (2006), it was used as partial replacement 15% by weight of cement in the mortar mixtures. The S.F. had an average particle size of 0.1 micrometer and a silicon dioxide content of 93%.

2.1.3 Fine aggregates

Natural siliceous sand with a fineness modulus of 2.91, a saturated surface dry specific gravity of 2.51 and absorption of 0.50 percent was used in the present experimental work.

Fig. 4 Wire mesh tensile test

2.1.4 Chemical admixtures (Super plasticizer)

Super plasticizer complies with ASTM C494 type F, and B.S. 5075 part 3, with a specific weight of 1.2 at 20ºC was used to provide the necessary workability for concrete and mortar. The super plasticizer's commercial name is SIKAMINT 163M. The manufacturer recommended dosage is between 0.5-2 percent by weight of cementatious materials.

2.1.5 Synthetic fibers

Synthetic fibers were added to the mortar mix of the ferrocement laminate for all the tested specimens incorporating ferrocement forms. The added fibers, are commercially as "fiber mesh 300". According to the manufacturer published data, this type of fibers is 100 percent virgin homopolymer polypropylene fibrillated fibers containing no reprocessed olefin materials. This type of fibers is specifically engineered and manufactured in an ISO 9001:2000 certified facilities to an optimum gradation for use as concrete secondary reinforcement at a minimum of 0.1% by volume (0.9 kg/m^3). The fibers comply with National Building Codes and ASTM C III6/C III6M, Type III fiber reinforced concrete (2015).

2.1.6 Reinforcing steel bars

High tensile deformed steel bars of diameter 10 mm were used to reinforce the control columns. Tensile tests were performed on three samples of the bars. The average test results of the three samples showed the proof stress and ultimate strength of the material were 551 MPa and 670 MPa respectively. Mild steel stirrups of diameter 6 mm were used as shear reinforcement for the control column. The material has nominal yield stress of 240 MPa.

2.1.7 Expanded steel mesh

Expanded steel mesh of diamond size 32×14 mm, weight equal 1660 gm/m^2 and dimensions of wire 1.25×1.5 mm was used as reinforcing materials as shown in Fig. 2(a). Three samples of mesh were tested using the Universal Testing Machine as shown in Fig. 4 to investigate the mechanical properties. The mesh has a proof stress of 199 MPa, ultimate strength of 320 MPa, and modulus of elasticity 120 GPa.

2.1.8 Welded steel mesh

Welded square galvanized steel mesh of dimensions 12.5 mm×12.5 mm and 600 gm/m^2 was employed as shown in Fig. 2(b). The mechanical properties were obtained experimentally as illustrated previously in Fig. 4. The mesh has a proof stress of 737 MPa and ultimate strength of 834 MPa and modulus of elasticity 170 GPa.

2.1.9 Polyethylene Mesh

This type of mesh is made from high density polyethylene. "Geogrid CE 121" was used for this type of mesh as shown in Fig. 2(e). The mesh has opening size of 6x8 mm, thickness of 3.3 mm, and weight of 725 gm/m^2 and volume fraction of 2.04%. Tensile test was performed on the mesh and the results showed that this type of polyethylene mesh has strength of 24.7 MPa and extension of 21%.

2.1.10 Fiber glass mesh

Gavazzi "V3-133-A" was used for this type of mesh. Mesh has opening dimension of 12.5×11.5 mm. The cross section dimension of the fiber strings in the longitudinal direction is 1.66×0.66 mm and in the transverse direction is 1.0×0.5 mm as shown in Fig. 2(d). The mesh has weight of 123 gm/m^2 and volume fraction of 0.535%. The tensile test on this type of mesh showed that it has tensile strength in the longitudinal direction of 325 MPa and extension of 5.5%.

2.2 Mix design

The materials used for the mix design were ordinary Portland cement, sand, silica fume and a super plasticizing agent. The main objectives of mix design was to determine the high amount of cement could be partially replaced by silica fume to increase strength of mortar matrix with no detrimental effects on the quality and properties of the mix in both the fresh and hardened states. The requirement of good workability was essential, to allow the mortar matrix to penetrate through the layers of steel mesh reinforcement. A super plasticizing agent was used to increase flow characteristics and accelerate the early strength development. Mortar mixtures for the ferrocement were made using a water to cement ratio of 0.4, sand to cement ratio of 2:1 and super-plasticizer of 2% by weight of cement, while 10% by weight of cement was replaced by S.F. The density of the mortar mix was approximately 2200 kg/m^3. The average compressive strength after 28 days was 35 MPa.

2.3 Mechanical properties of mixes

All mixes were performed using mechanical mixer. For all mixes, the constituent materials were first dry mixed; then, the mix water was added during mixing. Mechanical compaction was applied for all specimens using a mechanical vibrator. The values of the average compressive strength of the concrete and mortar are shown in Table 2.

2.4 Preparation of test specimens

The cages of the twelve columns using steel bars combined with metallic and non metallic meshes were prepared. The molds used for casting the test specimens

Table 2 Compressive strength of the concrete mortar

Designation	Average Ferrocement Mortar Compressive Strength (MPa)
Columns C1, C2, C3, and C4	40
Columns C5, C6, C7, and C8	39
Columns C9 ,C10, C11, and C12	39

(a) columns C2, C3, C4 (b) columns C6, C7, C8, and C9

Fig. 5 Details of reinforcing materials of RC columns ready for casting

were placed on a vibrating table to assure good compaction of ferrocement mortar as shown in Fig. 5. The wooden molds were disassembled on the next day and the specimen was weighed. The specimens were placed in the curing room for 28 days.

3. Finite element simulation

Nonlinear finite element analysis; (NLFEA) was carried out to investigate the behavior of the reinforced concrete columns using innovative composites specimens employing ANSYS-10.0 Software (2005). The investigated behavior includes the cracks pattern, the ultimate load and the load-vertical displacement response of the test specimens. Measurements were taken on central 200 mm length of the column, same as laboratory measurements. In addition, extensive non linear finite elements analysis had been conducted to investigate in deep the behaviour of the concrete columns reinforced by innovative composites.

Solid65 elements were used for modelling mortar and the wire meshes. Each element is defined by eight nodes. Each node has three degrees of freedom (translations in the nodal *x*, *y*, and *z* directions). This element has one solid material and up to three rebar materials in the three directions. The solid material is used to model the mortar. The rebar capability is used for modelling wire mesh. The wire mesh is specified by its material, volume ratio and orientation angles. The volume ratio is defined as the rebar volume divided by the total element volume. The orientation is defined by two angles in degrees (θ and φ) from the element coordinate system as shown in Fig. 6. This element has the ability of cracking (in the three orthogonal directions), crushing, plastic deformation, and creep as discussed by Hoque (2006), Singh (2006), Shaheen *et al* (2013). An eight-node solid element, Solid 45, was used to model the steel plates under the load. The element is defined with eight nodes having three degrees of freedom at

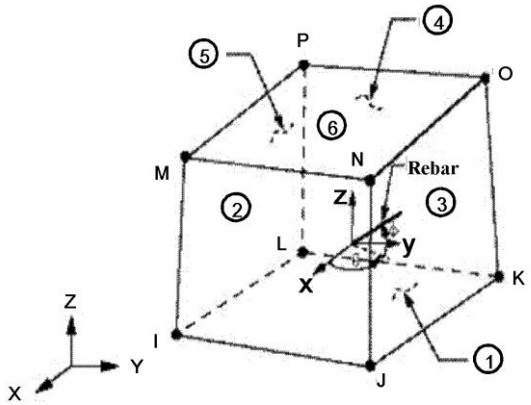

Fig. 6 Solid65-3D solids modeling

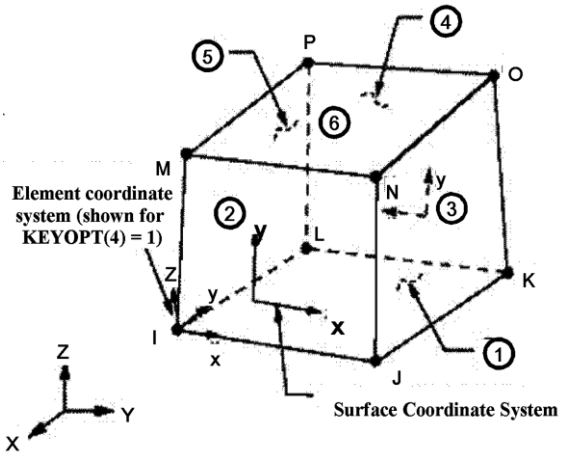

Fig. 7 Solid45-3D solids modeling

each node in the nodal x, y, and z directions. The geometry and node locations for this element type are shown in Fig. 7. Steel bars and stirrups were modelled by link8 elements. Link8 is a uniaxial tension-compression element with three degrees of freedom at each node: translations in the nodal *x*, *y*, and *z* directions. Plasticity, creep, swelling, stress stiffening, and large deflection capabilities are included. A schematic of the element was shown in Fig. 8.

Each support was presented by 25-hinged supports. The load was concentrated at the top end of the analyzed columns as indicated in Fig. 9.

The material of the mortar is defined by the compressive, tensile strength of concrete after 28 days, the modulus of elasticity and the multi-linear isotropic stress-strain curve. The modulus of elasticity of concrete and stress-strain curve were employed the Egyptian Code (2007). The modulus of elasticity of concrete (E_c in MPa) can be calculated from Eq. (3) by considering the compressive strength of concrete after 28 days (F_{cu} in MPa). The multi-linear isotropic stress- strain curve for the concrete can be computed by Eq. (4). The modulus of elasticity of concrete is considered as 14 GPa. The steel and the wire meshes were defined by the yield stress and the modulus of elasticity as illustrated in the material properties section.

$$E_c = 4400\sqrt{F_{cu}} \quad (3)$$

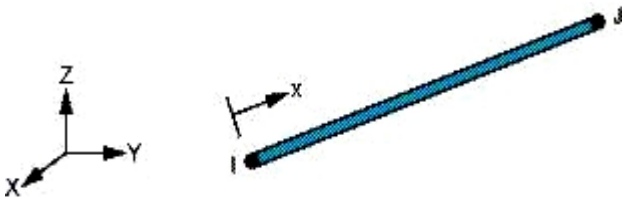

Fig. 8 Link8-3D spar modeling

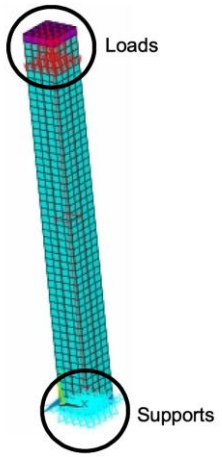

Fig. 9 FE simulation of the tested column C10

$$stress = \frac{E_c \varepsilon}{1+(\varepsilon / \varepsilon_o)^2} \quad (4)$$

$$\varepsilon_o = \frac{2F_{cu}}{E_c} \quad (5)$$

4. Results and discussion

4.1 Experimental results

In what follows the performance of the reinforced concrete columns reinforced with different innovative composite materials is presented and discussed. The compression strength behaviour was investigated including the load-carrying capacity, the cracking pattern, the failure mode and finally the specimen's deformation and strains.

All test specimens were tested under concentric compression loadings and readings for deformation over a gauge length of 200 mm versus the applied load were recorded using data acquisition system to construct load-deformation curves.

4.1.1 Ultimate capacity

Table 3 shows first crack load and ultimate loads for all the tested columns. The failure load of the control specimen; C1 is shown in Table 2 was 304 kN. For specimen C2, the failure load was 306.8 kN indicating slightly enhancement in the ultimate capacity. The enhancement in the load-carrying capacity was 0.92%. For specimens C3, the increase in the ultimate capacity reached

Table 3 1st crack and ultimate load results for all test specimens

Designation	Volume Fraction (%)	First Crack load (kN)	Ultimate Load (kN)	Load-Carrying Capacity Enhancement (%)
C1	3.8560	115.4	304.0	-------
C2	0.7337	215.5	306.8	0.92
C3	3.8776	232.0	330.0	8.55
C4	1.4674	223.0	340.0	14.47
C5	4.6113	236.8	370.0	21.71
C6	0.5350	251.8	420.0	38.16
C7	3.6789	333.3	485.4	59.67
C8	1.0700	315.5	481.7	58.45
C9	4.2139	364.5	506.4	66.58
C10	4.2019	237.5	320.5	5.43
C11	3.7920	195.0	217.9	-28.32 (no enhancement)
C12	5.4720	253.7	288.5	-5.10 (no enhancement)

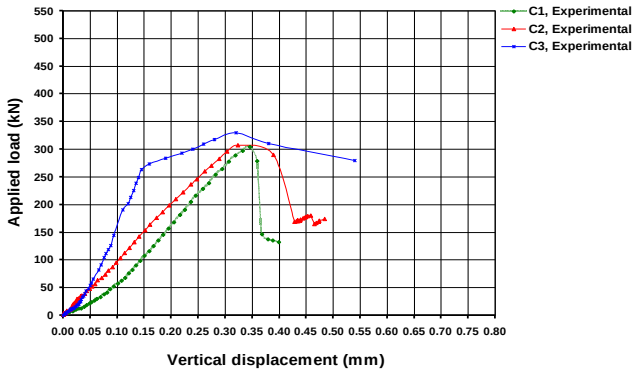

Fig. 10 Load - vertical displacement curves for series C1 to C3

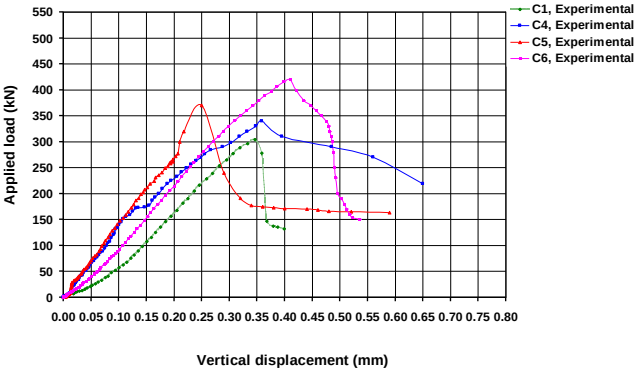

Fig. 11 Load - vertical displacement curves for series C4 to C6

8.55%. For the specimen C4, the failure load was 340.0 kN with an enhancement of 14.47%. For the specimen reinforced with two layers of expanded wire mesh with four longitudinal steel bars each has a diameter 10 mm, C5, the experimental failure load was 370.0 kN with a significant enhancement of 21.71% in the ultimate capacity. For C6, C7, C8, and C9, the failure loads were 420.0 kN, 485.4 kN, 481.7 kN, and 506.4 kN, with a big significant enhancement

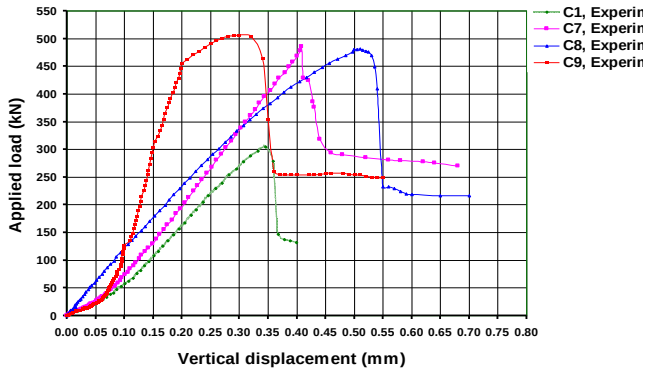

Fig. 12 Load - vertical displacement curves for series C7 to C9

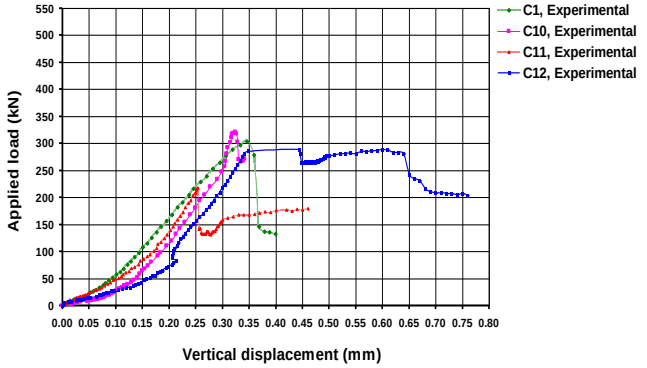

Fig. 13 Load - vertical displacement curves for series C10 to C12

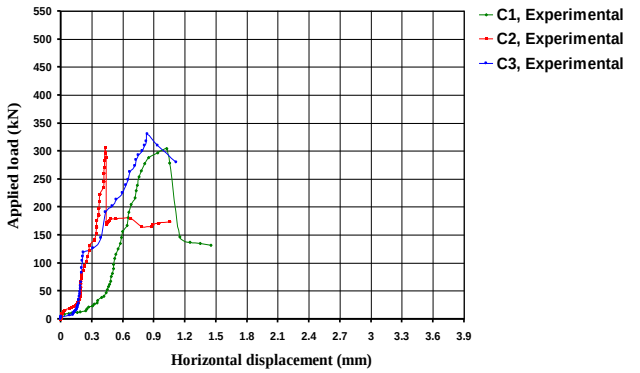

Fig. 14 Load - horizontal displacement curves for series C1 to C3

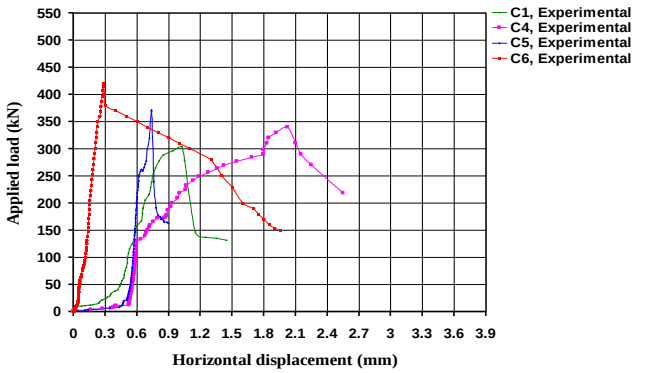

Fig. 15 Load - horizontal displacement curves for series C4 to C6

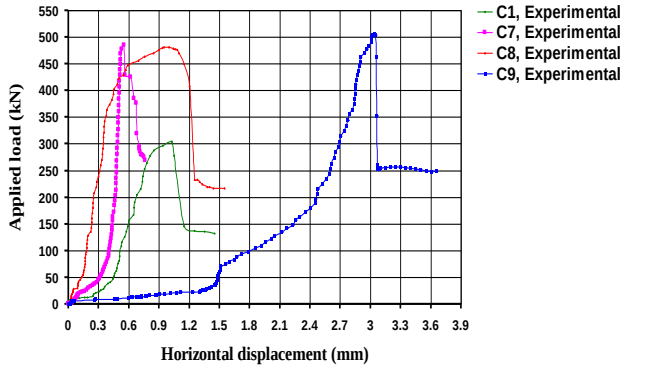

Fig. 16 Load - horizontal displacement curves for series C7 to C9

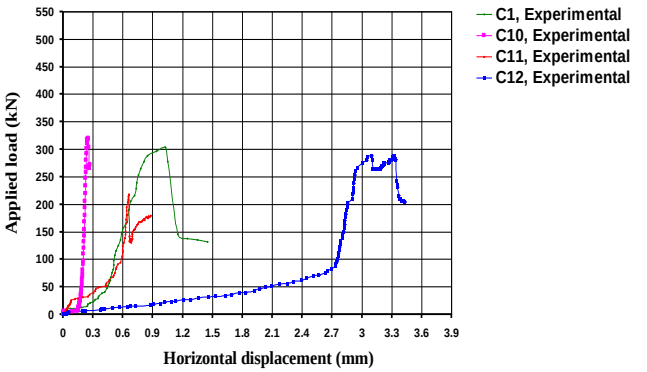

Fig. 17 Load - horizontal displacement curves for series C10 to C12

of 38.16%, 59.67%, 58.45%, and 66.58% respectively. For C10, the failure load was 320.5 kN, with an increase of 5.43% in the ultimate capacity. For the specimen reinforced with one layer of fiber glass mesh with four longitudinal steel bars each has a diameter 10 mm and stirrups, C11, the failure load was 217.9 kN with a reduction of 28.32% in the ultimate capacity. For C12, the failure load was 288.5 kN, with a reduction in the ultimate capacity of 5.10%. According to the results in Table 3, the effect of using welded wire mesh is more effective in enhancing the ultimate capacity than the other various types of metallic and non metallic mesh reinforcement.

Figs. 10 to 13 show the comparisons between load-vertical displacement curves of the tested specimens for series C1 to C3, C4 to C6, C7 to C9, and C10 to C12 respectively, while Figs. 14 to 17 show the comparisons between load-horizontal displacement curves of the tested specimens for series C1 to C3, C4 to C6, C7 to C9, and C10 to C12 respectively, in order to avoid sudden uncontrolled lateral displacement of a column at which point no additional load can be supported.

Also, Fig. 18 indicates the enhancement percentage in experimental carrying load capacity for different specimens.

4.1.2 Cracking

The first cracks in control specimen C1 started at load of

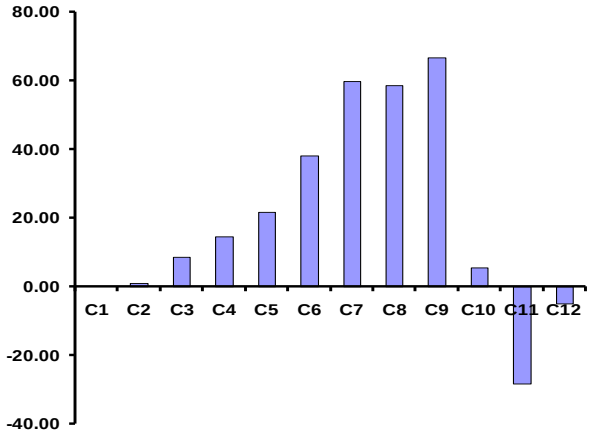

Fig. 18 Enhancement percentage in experimental carrying capacity

Table 4 Deformation characteristics of tested columns

Designation	Volume Fraction (%)	1st crack load (P_{FC}, kN)	Serviceability load (*) (P_{ser}, kN)	Ultimate load (P_{ult}, kN)	Ductility ratio	Energy Absorption (kN.mm)
C1	3.8560	115.4	189.79	304.0	2.44	58.29
C2	0.7337	215.5	191.54	306.8	2.01	90.07
C3	3.8776	232.0	206.04	330.0	4.00	134.48
C4	1.4674	223.0	217.29	340.0	2.17	151.96
C5	4.6113	236.8	231.04	370.0	3.31	108.60
C6	0.5350	251.8	262.29	420.0	2.46	126.07
C7	3.6789	333.3	303.17	485.4	2.31	167.52
C8	1.0700	315.5	300.85	481.7	1.97	190.76
C9	4.2139	364.5	316.29	506.4	3.12	156.09
C10	4.2019	237.5	200.10	320.5	1.23	38.72
C11	3.7920	195.0	135.98	217.9	1.91	54.57
C12	5.4720	253.7	180.10	288.5	2.26	142.11

(*) $P_{ser} = \frac{(P_{ult} - 1.4 * D.L.)}{1.6}, D.L. = own\ \ weight\ \ of\ \ column.$

115.4 kN at the column head under the point of load concentration, and then propagated suddenly at the maximum load of 304 kN. After this, the load decreases and the cracks increased showing the failure of column.

For specimens C2, C3, C4, C5, C6, C7, C8, C9, C10, C11 and C12, the recorded first crack load showed increased about 86.7%, 101.0%, 93.2%, 105.2%, 118.2%, 188.8%, 173.4%, 215.9%, 105.8%, 69.0%, and 119.8% respectively. This indicates the capability of the welded wire mesh than the other techniques.

Generally, the cracks for all tested columns started at later stage of loading indicating better confinement and better serviceability. However, for different types of innovative composite, the ultimate strength increased and the cracks slightly increased in length and width to different extent, as shown in Fig. 19 (a to h) and Table 4.

4.1.3 Modes of failure

Near failure, the control specimen column failed in a mode of compression failure accompanied with local crushing and spalling of the concrete cover. For the other

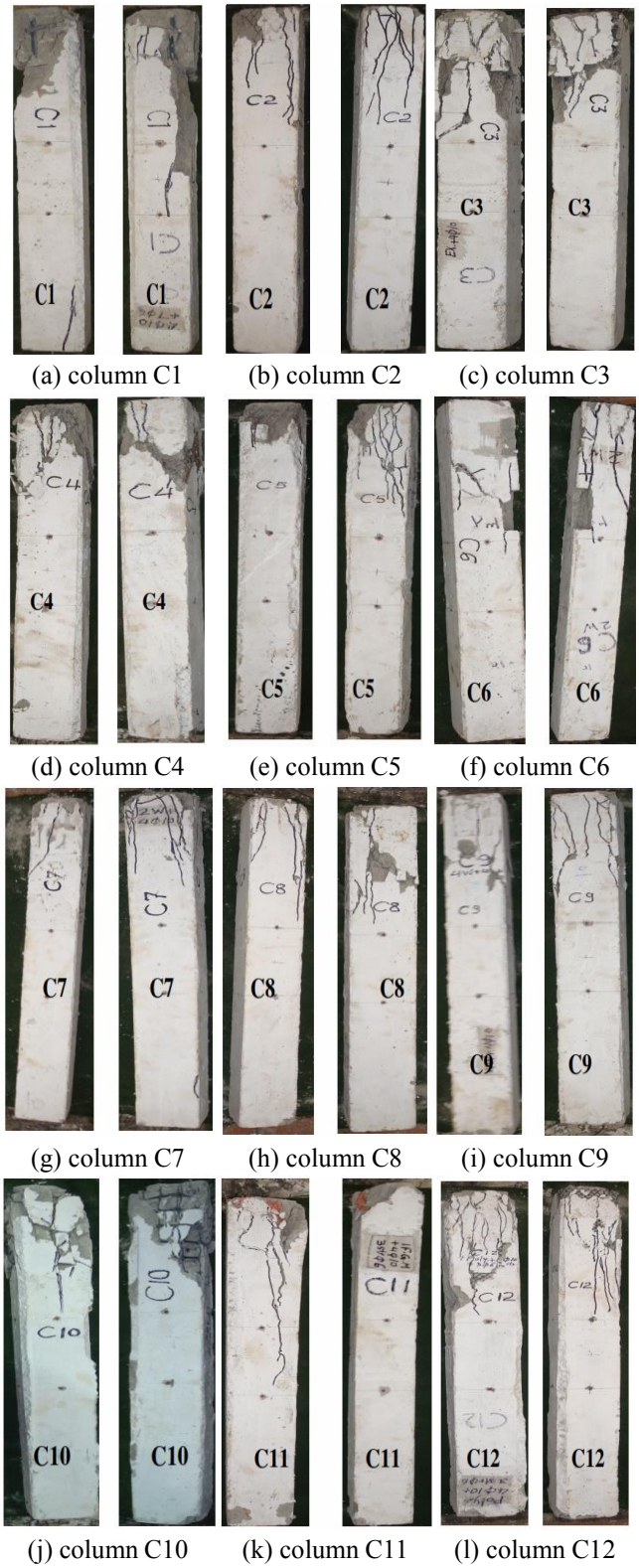

(a) column C1 (b) column C2 (c) column C3

(d) column C4 (e) column C5 (f) column C6

(g) column C7 (h) column C8 (i) column C9

(j) column C10 (k) column C11 (l) column C12

Fig. 19 Cracking patterns for all test specimens

series of the tested specimens, near failure the load reach the maximum value and after this value the load decreased up to 70% to 50% of the maximum load with increasing the descending part of load displacement curves. This indicates the increases of the service load which represent the safe line in using the structures as shown in Table 4 and Fig. 20.

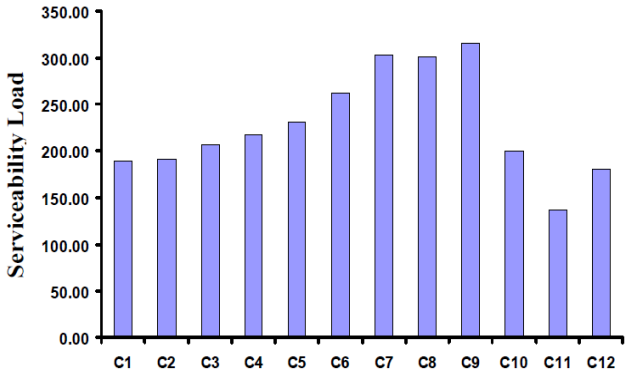

Fig. 20 Serviceability loads in function of tested specimen type

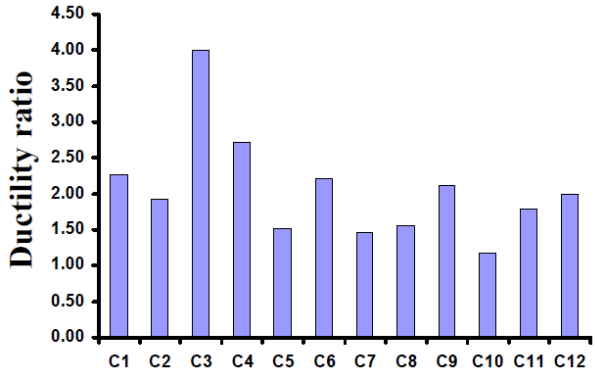

Fig. 21 Ductility ratios in function of tested specimen type

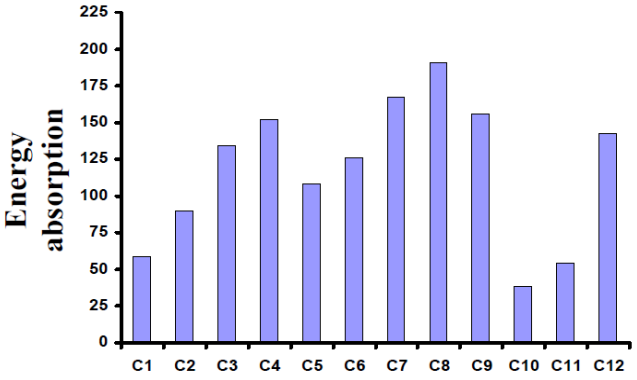

Fig. 22 Energy absorption in function of tested specimen type

4.1.4 Ductility and energy absorption

Ductility ratio was defined as the ratio of the maximum deformation at ultimate load to that at the first crack load, while energy absorption was defined as the area under the load-deformation curve up to failure. Table 4 shows the values of the ductility ratios and energy absorption of all the tested columns. Progressive increase of energy absorption with volume fraction percentage was observed. Fig. 21 shows comparison of the ductility ratio values for all tested specimens. It is observed that the column C3, which use one layer of expanded steel mesh instead of the traditional reinforcement (steel bars and stirrups), with four longitudinal steel bars, each has a diameter 10 mm, has a

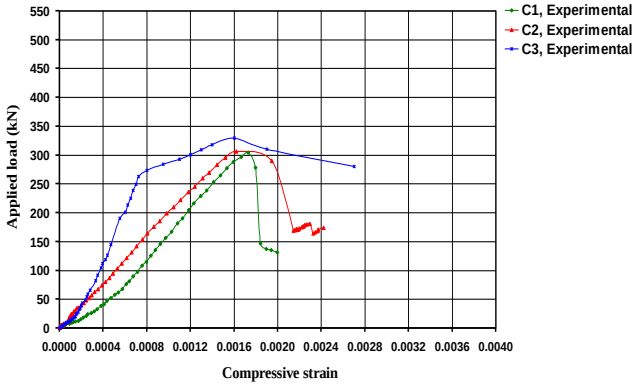

Fig. 23 Load - compressive strain curves for series C1 to C3

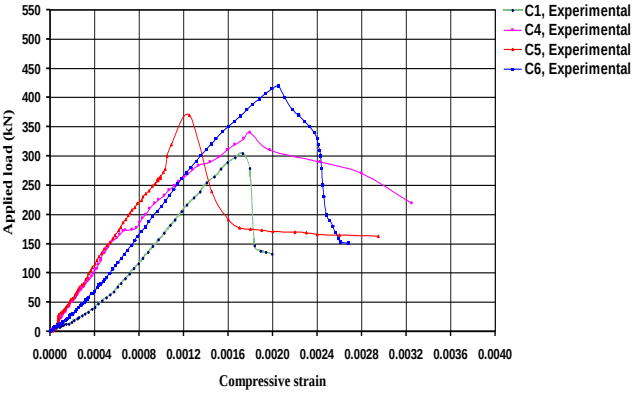

Fig. 24 Load - compressive strain curves for series C4 to C6

maximum ductility ratio. Fig. 22 shows comparison of the energy absorption values for all tested specimens.

It is cleared that the column C8, which use four layer welded steel mesh, has a maximum energy absorption.

It can be concluded that using these innovative composites enhanced the behaviour of failure by increasing the ductility ratio. Finally, using these innovative composite materials enhanced the behaviours of the tested columns. It can be state that it delayed the appearance of the first cracks and increased the service load capacity. In addition, it developed with high ultimate loads, crack resistance, better deformation characteristics, high durability, high ductility and energy absorption properties, which are very useful for dynamic applications.

4.1.5 Compressive strain

Figs. 23 to 26 show the comparisons between compressive strain curves of the tested specimens for series C1 to C3, C4 to C6, C7 to C9, and C10 to C12 respectively. Table 5 shows compressive strains at first crack and ultimate loads of all the tested columns, while Figs. 27 and 28 show comparison of the compressive strains at first crack and ultimate loads respectively.

It can be concluded that the specimen C2, which reinforced with one layer expanded steel mesh, has a maximum compressive strain at first and ultimate loads respectively. This is due to this tested specimen has a lowest amount of reinforcement, in comparison to the other columns.

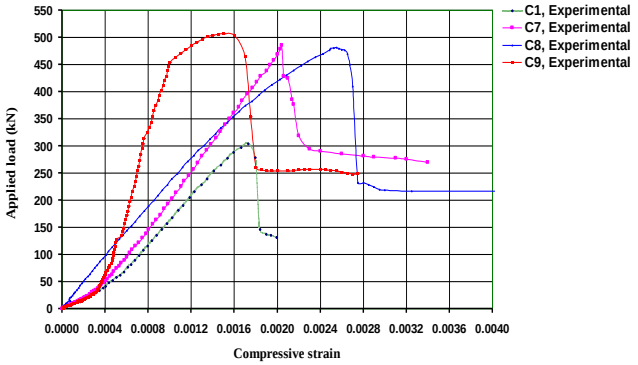

Fig. 25 Load - compressive strain curves for series C7 to C9

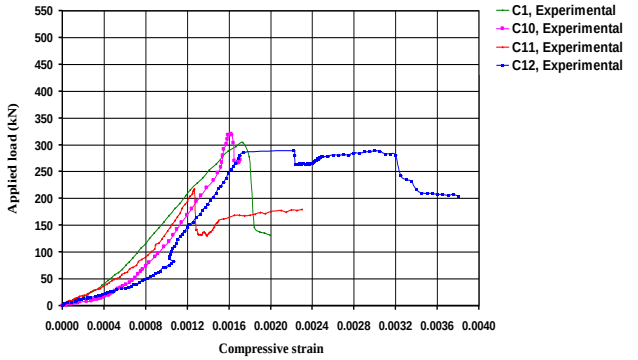

Fig. 26 Load - compressive strain curves for series C10 to C12

Table 5 Compressive strain at 1st crack and ultimate loads of tested columns

Designation	Volume Fraction (%)	Compressive strain at 1st crack load ($\times 10^{-4}$)	Compressive strain at ultimate load ($\times 10^{-4}$)
C1	3.8560	6.95	11.30
C2	0.7337	14.05	22.80
C3	3.8776	11.60	14.00
C4	1.4674	10.60	16.95
C5	4.6113	8.70	12.50
C6	0.5350	11.05	18.50
C7	3.6789	8.90	15.40
C8	1.0700	10.90	17.50
C9	4.2139	8.50	13.00
C10	4.2019	11.60	14.20
C11	3.7920	9.00	12.70
C12	5.4720	9.60	13.20

4.2 Comparison between experimental and FE simulation results

The comparison between experimental and FE simulation results; include 1st crack load, serviceability load, ultimate load, cracking patterns, curves of load–vertical displacement, and ductility ratio.

4.2.1 Ultimate load carrying capacity

Good agreement between the nonlinear finite element

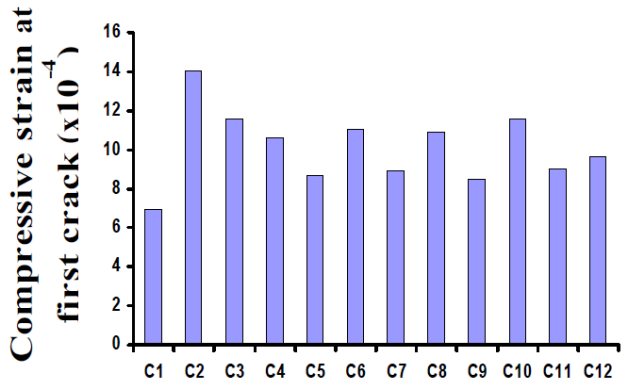

Fig. 27 Compressive strain in function of tested specimen type at 1st crack

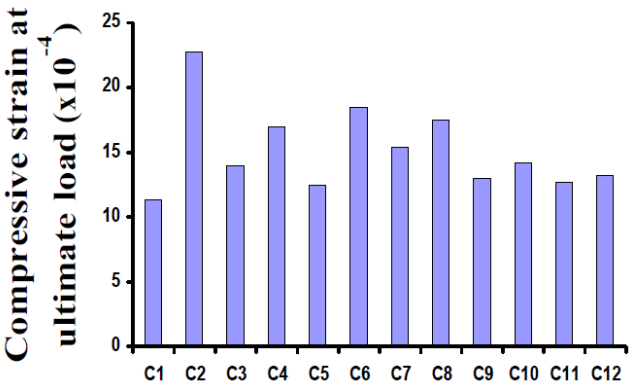

Fig. 28 Compressive strain in function of tested specimen type at ultimate load

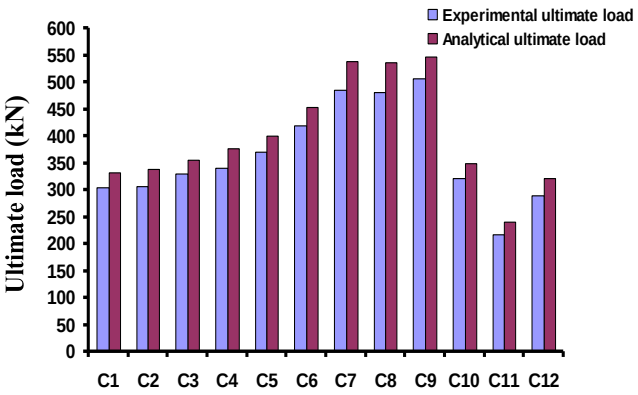

Fig. 29 Failure load of selected models with varying column

analysis (NLFEA) predictions and the recorded load-carrying capacity is shown in Fig. 29 and Table 6. For the control specimen C1, the analytical ultimate load to the experimental load; $P_{ult(NLFEA)}$ / $P_{ult(EXP.)}$ was equals to 1.09. For other specimens, the ratio of the analytical ultimate load to the experimental load; $P_{ult(NLFEA)}$ / $P_{ult(EXP.)}$ ranges between 1.08 and 1.11 with a mean value of 1.095, refer to Table 6 for the result.

Furthermore, the analysis reflected the strengthening significance. The comparison between the experimental and the analytical enhancement values in ultimate load capacity P_u was as shown in Fig. 30.

Table 6 Comparison of the experimental and FE 1st crack and ultimate loads for tested columns

Designation	Initiation of crack P_{FC} (kN)		Ultimate load P_{ult} (kN)		$P_{FC\ (NLFEA)}$ / $P_{FC\ (EXP)}$	$P_{ult\ (NLFEA)}$ / $P_{ult\ (EXP)}$
	EXP.	NLFEA	EXP.	NLFEA		
C1	180.40	140.65	304.0	331.0	0.78	1.09
C2	215.50	140.65	306.8	339.0	0.65	1.10
C3	232.00	140.65	330.0	356.0	0.61	1.08
C4	223.00	140.65	340.0	376.0	0.63	1.11
C5	236.80	140.65	370.0	399.0	0.59	1.08
C6	251.80	140.65	420.0	454.0	0.56	1.08
C7	333.30	140.65	485.4	539.0	0.42	1.11
C8	315.50	140.65	481.7	536.0	0.45	1.11
C9	364.50	140.65	506.4	547.0	0.39	1.08
C10	237.50	140.65	320.5	349.0	0.59	1.09
C11	195.00	140.65	217.9	241.0	0.72	1.11
C12	253.70	140.65	288.5	321.0	0.55	1.11

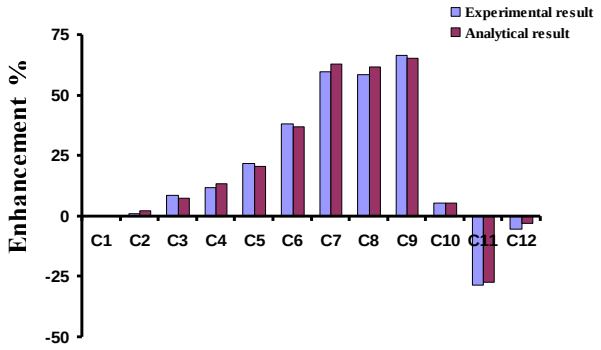

Fig. 30 Enhancement percentage in experimental and analytical carrying capacity

4.2.2 Cracking behavior

The cracking was initiated at early loading stage in the concrete elements modeling the loaded face of the column nearby the supporting of columns as shown in Fig. 31. Referring to Table 6, the experimental cracking capacity is shown to be vary from 180.4 kN for specimen C1, and 364.9 kN for specimen C9, being somewhat independent

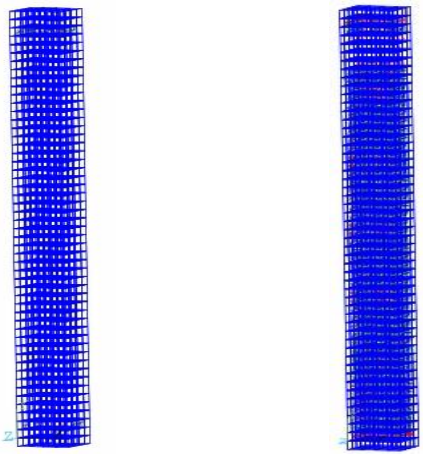

(a) 1st cracks (b) all cracks

Fig. 31 First and all cracks of control specimen

on the reinforcing characteristics. This early stage of crack loading is due to the unseen micro cracks in experimental test. The cracking load, as such, is quite below the experimental cracking capacity. The ratio of the analytical cracking load to the experimental load. $P_{FC(NLFEA)}$ / $P_{FC(EXP)}$ is shown to be ranged from 0.39 to 0.78 with a mean value of 0.59 as indicated in Table 6.

This is may be justified as the NLFEA predictions represent the micro-cracking stage which precedes the visible cracking stage. Moreover, the innovative composites materials might have concealed the micro cracks developed underneath in the experiments.

On the other hand, the cracking patterns at each load increment revealed that propagation of the cracks for all specimens was slightly different with respect to the experimental crack pattern.

This is due to the accuracy of the non linear finite element program in determined the micro cracks and wide cracks, and reflected the significance of the reinforcing method on the cracking patterns as shown in Table 6. The comparison of the crack patterns for the experimental and the analytical cases is illustrated as shown in Fig. 32(a) to (m).

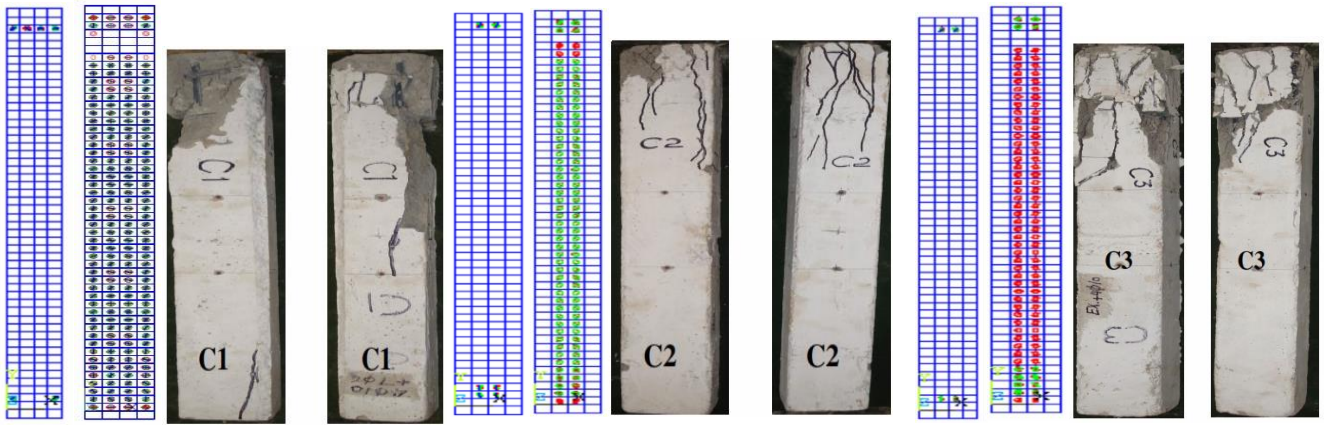

(a) column C1 (b) column C2 (c) column C3

Fig. 32 Experimental and analytical crack patterns for all columns

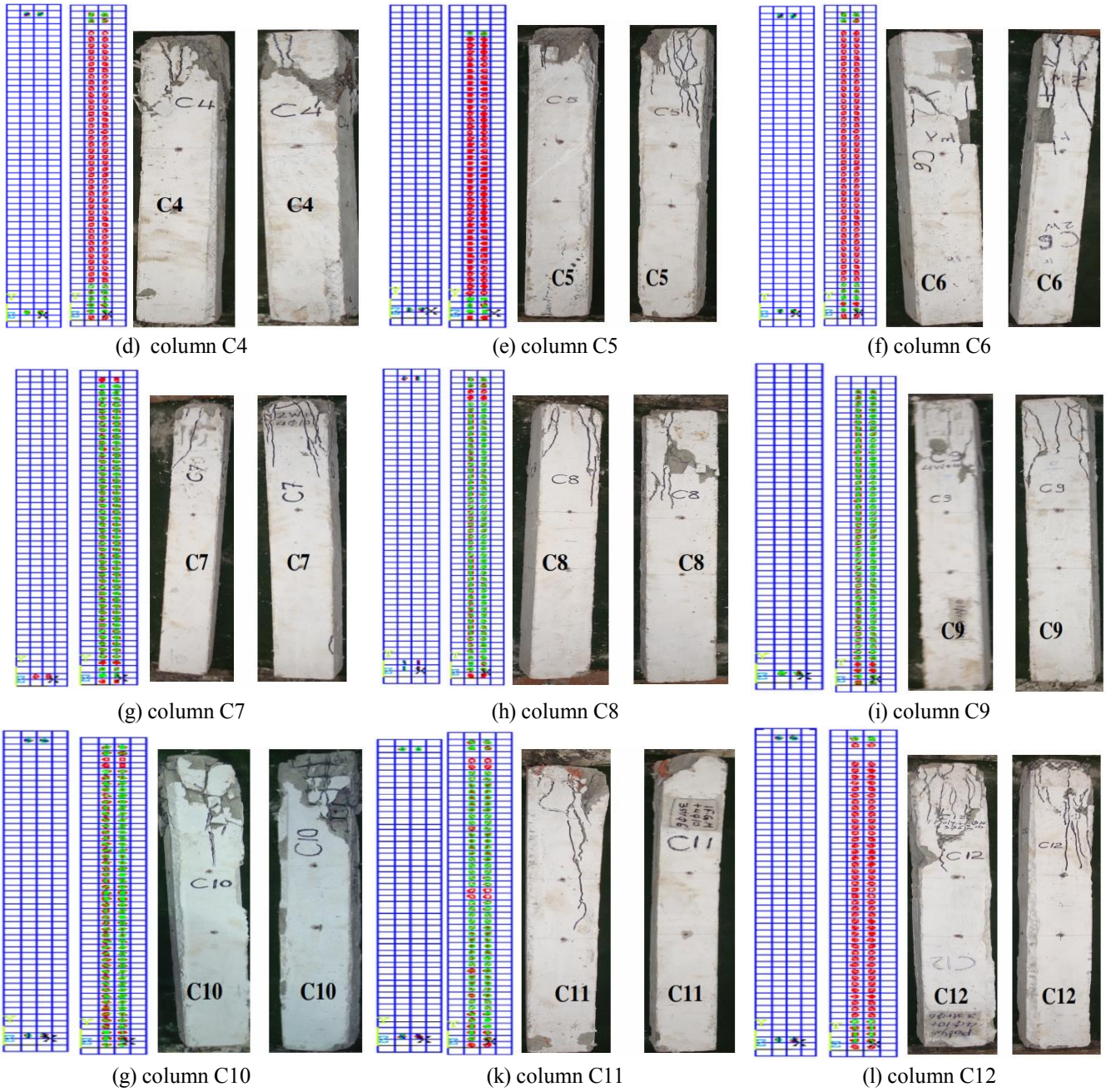

(d) column C4 (e) column C5 (f) column C6

(g) column C7 (h) column C8 (i) column C9

(g) column C10 (k) column C11 (l) column C12

Fig. 32 Continued

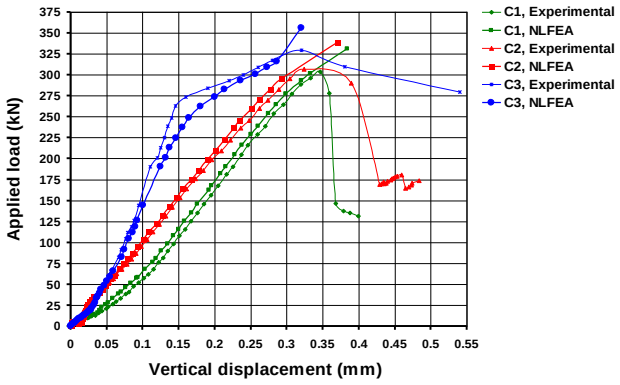

Fig. 33 Curve applied load in function of vertical displacement of experimental and proposed models C1, C2, and C3

4.2.3 Deformation characteristics

Figs. 33 to 40 present the load-vertical displacement curves; and also the load-horizontal displacement curves, as obtained from the experimental and theoretical approaches for the all test composite columns. Good agreement is observed between the theoretical and experimental results as shown.

Figs. 41 and 42 show the comparison of the compressive strains for the experimental and the analytical cases at 1st crack and ultimate loads respectively. It can be concluded that the FE simulations give accurate results in comparing with the experimental results. In addition, the analytical compressive strain results experience greater than the experimental results by a mean value of 11% as shown.

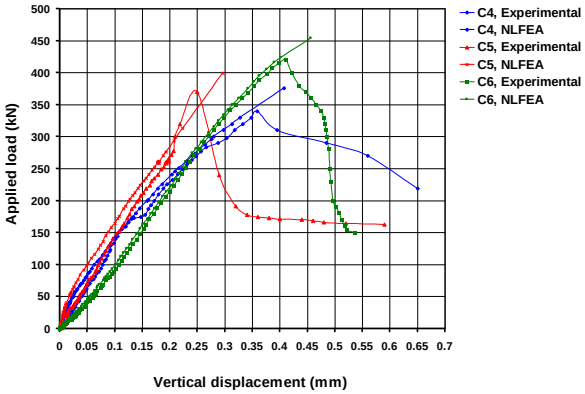

Fig. 34 Curve applied load in function of vertical displacement of experimental and proposed models C4, C5, and C6

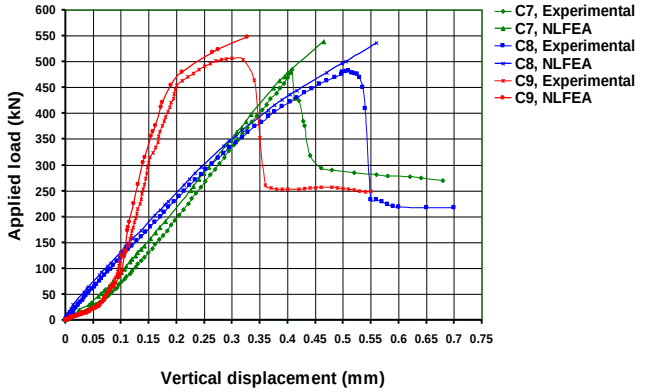

Fig. 35 Curve applied load in function of vertical displacement of experimental and proposed models C7, C8, and C9

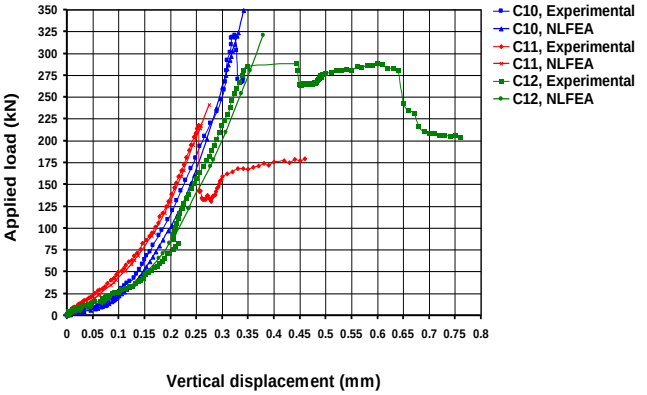

Fig. 36 Curve applied load in function of vertical displacement of experimental and proposed models C10, C11, and C12

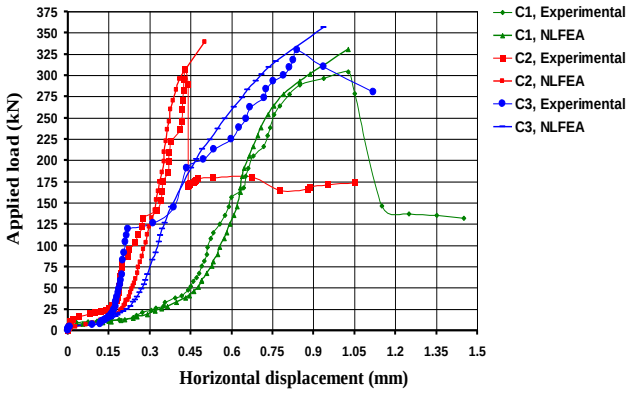

Fig. 37 Curve applied load in function of horizontal displacement of experimental and proposed models C1, C2, and C3

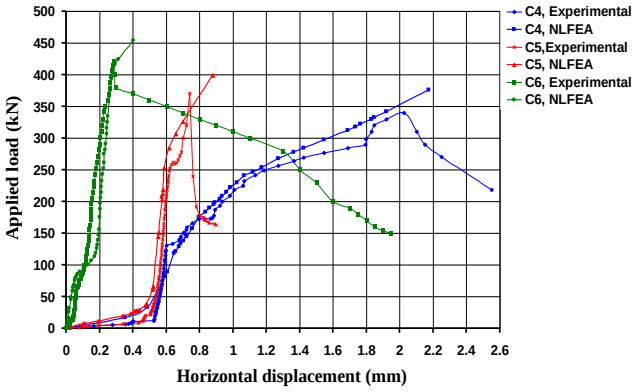

Fig. 38 Curve applied load in function of horizontal displacement of experimental and proposed models C4, C5, and C6

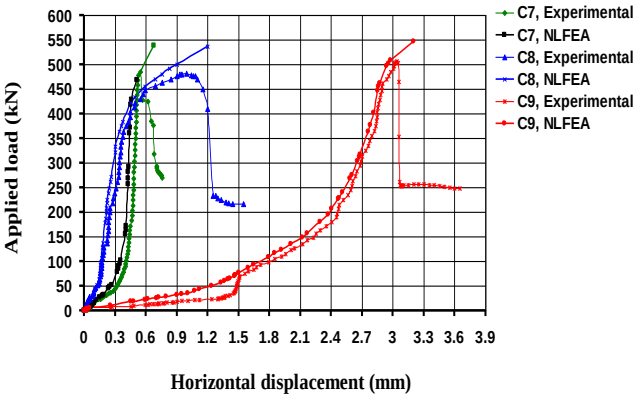

Fig. 39 Curve applied load in function of horizontal displacement of experimental and proposed models C7, C8, and C9

Fig. 43 shows the comparison of the ductility ratio for the experimental and the analytical cases at ultimate loads.

It has to be concluded that the experimental ductility ratio results experience less than the analytical results by a mean value of 10% as shown.

5. Parametric study

To further improve the understanding of the mechanical behavior of RC columns reinforced with composite materials, parametric studies were performed to investigate the impact of the increase of the column dimensions, upon the strength capacity of the models having ferrocement reinforcement.

The study was conducted on three proposed models. The first model has cross section dimensions of 150 mm×150

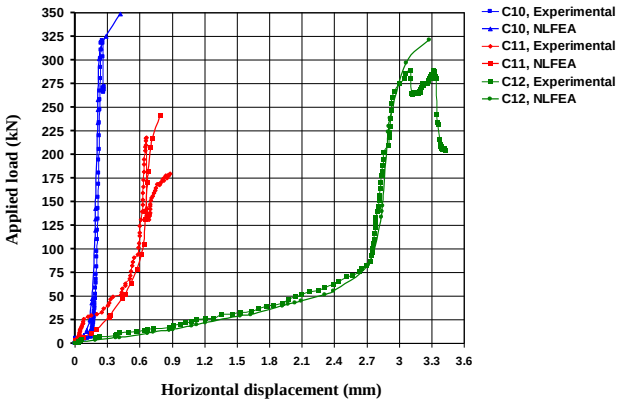

Fig. 40 Curve applied load in function of horizontal displacement of experimental and proposed models C10, C11, and C12

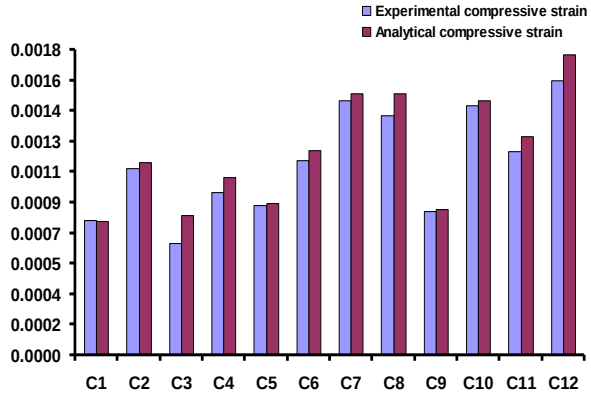

Fig. 41 Compressive strain in function of specimen type at 1st crack

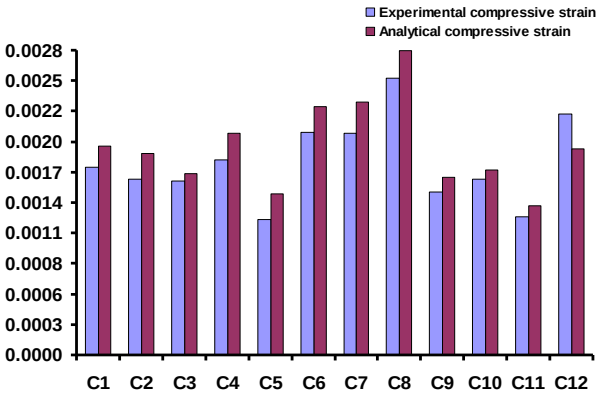

Fig. 42 Compressive strain in function of specimen type at ultimate load

mm and length of 1500 mm. The second has cross section dimensions of 200 mm×200 mm and has length of 2000 mm, while the third model has cross section dimensions of 250 mm×250 mm and has length of 2500 mm.

Fig. 44 compares the results obtained for the ultimate load values. It has to be observed that in case of an increase of the column dimensions by an amount of 50%, the FE ultimate load increase by a mean value of 60%, according to the reinforcement type of composite column.

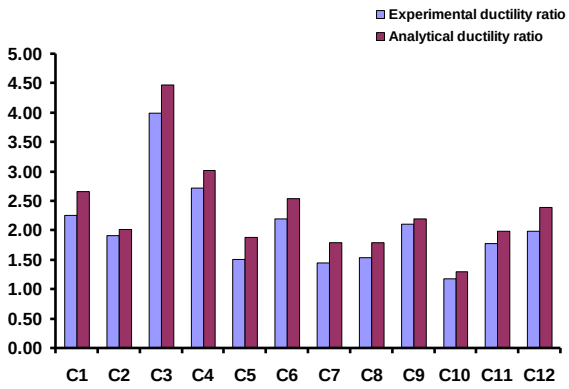

Fig. 43 Ductility ratio in function of specimen type at ultimate load

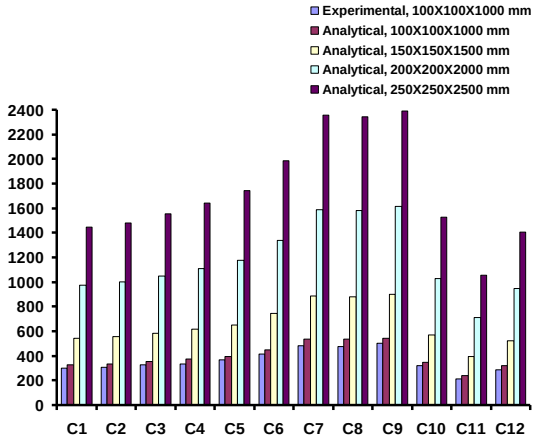

Fig. 44 Ultimate load in function of specimen type with varying column size

6. Conclusions

Based on the results and observations of the experimental and the analytical study presented in this study, and considering the relatively high variability and the statistical pattern of data, the following conclusions can be drawn:

1. Irrespective of the steel mesh type, expanded or welded volume fraction of steel reinforcement, ferrocement specimens tested under axial compression loadings exhibit superior ultimate loads compared to the control ones.
2. Increasing in the volume fraction does not have much effect under axial compression loading in which the failure load is mainly governed by the spalling of the mortar cover around the steel reinforcement.
3. Changing steel mesh types, expanded or welded have much effect on ultimate loads under axial compression loading. There is higher strength gain of specimens reinforced with welded steel mesh about 41% compared with those reinforced with expanded steel mesh.
4. The test results show that the welded wire mesh exhibited a higher ultimate load than conventionally reinforced control columns by about 67% as indicated by column C9, which was reinforced with four layers of welded steel mesh in addition to four longitudinal steel

bars each has 10 mm. Therefore, there is strength gain about 67% by employing galvanized welded steel mesh as reinforcement.

5. Comparing the results of ultimate load in case of column C4 which was reinforced with two layers of expanded steel mesh and Column C8 which was reinforced with four layers of welded steel mesh, the percentage of increase is equal 41.7%. Superior high ultimate load and strength gain could be obtained by using welded steel mesh as reinforcement.

6. Column C9 which was reinforced with four layers of welded steel mesh in addition to four steel bars of 10mm in diameter, exhibited the higher ultimate load compared with all the tested columns without spalling of concrete cover this is predominant.

7. Column C10 which was reinforced with one layer of tensar mesh in addition to four steel bars 10mm in diameter and also three stirrups, each has 6mm in diameter, showed the higher ultimate load compared with C11 and C12 which were reinforced with non metallic materials.

8. Experimental results revealed that increasing the volume fraction of steel reinforcement contributed to a slightly higher ultimate load. This is clear when comparing column C6 with column C8, which contained double mesh reinforcement. The ultimate compression of column C8 was higher than that of column C6 by about 14.7%. However, the increase in the steel volume fraction resulted in a much stiffer specimen.

9. It is interesting to note that there is no spalling of mortar cover for specimens C7, C8, C9, C11 and C12 is predominant. It is interesting to note that column C9 reached high ultimate load compared with all tested columns. Column C10 which was reinforced with non metallic one layer of tensar mesh in addition to four longitudinal steel bars of 10 mm in diameter and three stirrups arrived high ultimate load compared with columns C11 and C12. Therefore increasing volume fraction percentage to 1.75% has a dominant effect in delaying occurrence of the developed cracks with high protection against corrosion and high strength gain compared with those reinforced with metallic reinforcement.

10. Finite element model can be used to investigate the mechanical behavior of ferrocement RC columns reinforced with composite material, leading to a good agreement when comparing to available full-scale test data.

11. The comparison of the crack patterns obtained by the FE and experimental models leads to an identical crack propagation for the two approaches up to failure. The inclination of the failure surfaces and the concentration of cracks of all columns were the same in both patterns.

12. An increase in the FE strength capacity mean values of 10% compared to the experimentally available data was concluded, leading to a good agreement between them.

13. Parametric study was performed in order to look at the effect of changing the column dimensions on the strength capacity of the RC composite columns. It has to be observed that in case of an increase of the column dimensions by an amount of 50%, the FE ultimate load increase by a mean value of 60%, according to the reinforcement type of composite column.

References

Abdel-Naby, A. (2006), "Development of ferrocement U-shaped beams infilled with core materials", M.S. Thesis submitted to the American University in Cairo, Egypt.

Abdel-Tawab, A. (2006), "Development of permanent formwork for beams using ferrocement laminates", Ph.D. Thesis, submitted to Menoufia University, Egypt.

Ahmed, T., Ali, S.K.S. and Choudhury, J.R. (1994), "Experimental study of ferrocement as a retrofit material for masonry columns", *Proceedings of the Fifth International Symposium on Ferrcement*, Eds. Nedwell and Swamy, E& FN Spon, London.

ANSYS (2005), "Engineering analysis system user's manual", vol. 1&2, and theoretical manual. Revision 8.0, Swanson analysis system inc., Houston, Pennsylvania.

ASTM C III6/C III6M Standard Specification for Fiber-Reinforced Concrete (2015), ASTM International, 100 Barr Harbor Drive, PO Box C700, West Conshohocken, PA, 19428-2959 USA.

El-kholy, A.M. and Dahish, H.A. (2015), "Improved confinement of reinforced concrete columns", *Ain Shams Eng. J.*, **7**(2), 1-12.

Fahmy, E.H., Abou-Zeid, M.N., Shaheen, Y.B. and Gaafar, H. (2005), "Behavior of ferrocement panels under axial and flexural loadings", *Proceedings of the 33rd Annual General Conference of the Canadian Society of Civil Engineering*, GC-150-1 - GC-150-10.

Fahmy, E.H., Shaheen, Y.B. and Abou-Zeid, M.N. (2004), "Development of ferrocement panels for floor and wall construction", *5th Structural Specialty Conference of the Canadian Society for Civil Engineering*, ST218-1-ST218-10.

Fahmy, E.H., Shaheen, Y.B. and Korany, Y. (1999), "Environmentally friendly high strength concrete", *Proceedings of the 24th Conference on Our World in Concrete and Structures*, 171-178.

Fahmy, E.H., Shaheen, Y.B. and Korany, Y. (1999), "Repairing reinforced concrete columns using ferrocement laminates", *J. Ferrocem.*, **29**(2), 115-124.

Fahmy, E.H., Shaheen, Y.B., Abou-Zeid, M.N. and Gaafar, H. (2004), "Ferro-cement sandwich and cored panels for floor and wall construction", *Proceedings of the 29th Conference on Our World in Concrete and Structures*, 245-252.

Fahmy, E.H., Shaheen, Y.B., Ezzat, H., Abdelnaby, A.M. and Abou-Zeid, M.N. (2013), "Applying the ferrocement concept in construction of concrete beams incorporating reinforced mortar permanent forms", *Int. J. Concrete Struct. Mater.*, **8**(1), 83-97.

Hazem, R. (2009), "Non-metallic Reinforcement for the U-shaped ferrocement forms instead of the conventional steel mesh", *Deutsches Zentrum für Entwicklungstechnologien*.

Hoque, M. (2006), "3D nonlinear mixed finite-element analysis of RC beams and plates with and without FRP reinforcement", M.Sc. Thesis, University of Manitoba, Winnipeg, Manitoba, Canada.

Housing and Building national research Center (2007), "The Egyptian Code for Design and Construction of Concrete Structures", ECP 203-2007, Ministry of Housing, Utilities and Urban Communities, Giza, Egypt.

IFS Commitee 10 (2001), "Ferrocement model code: building code recommendations for ferrocement", IFS 10-01, *International Ferrocement Society*, Asian Institute of

Technology, Bangkok, Thailand.
Kaish, A.B.M.A., Jamil, M., Raman, S.N., Zain, M.F.M. and Alam, M.R. (2016), "An approach to improve conventional square ferrocement jacket for strengthening application of short square RC column", *Mater. Struct.*, **49,** 1025-1037.
Kaushik, S.K., Prakash, A. and Singh, K.K. (1994), "Inelastic buckling of ferrocement encased columns", *Proceedings of the Fifth International Symposium on Ferrcement*, Eds. Nedwell and Swamy, E& FN Spon, London.
Kumar, V. and Patel, P.V. (2016), "Strengthening of axially loaded concrete columns using stainless steel wire mesh (SSWM)-numerical investigations", *Struct. Eng. Mech.*, **60**(6), 979-999.
Kwon, M., Seo, H. and Kim, J. (2016), "Seismic performance of RC-column wrapped with Velcro", *Struct. Eng. Mech.*, **58**(2), 379-395.
Mansur, M.N. and Paramasivam, P. (1990), "Ferro-cement short columns under axial and eccentric compression", *ACI Struct. J.*, **84**(5), 523-529.
Nedwell, P.J., Ramesht, M.H. and Rafei-Taghanaki, S. (1994), "Investigation into the repair of short square columns using ferrocement", *Proceedings of the Fifth International Symposium on Ferrcement*, Eds. Nedwell and Swamy, E& FN Spon, London.
Onathara, M. and Martin, I.M. (2015), "Comparative study of columns strengthened by steel angles and ferrocement jacketing", *International Conference on Technological Advancements in Structures and Construction*, TASC- 15, 10-13.
Shaheen, Y.B.I., Eltaly, B. and Kameel, M. (2013), "Experimental and analytical investigation of ferrocement water pipe", *J. Civil Eng. Constr. Tech*., **4**(4), 157-167.
Shaheen, Y.B.I., Mahmoud, A.M. and Refat, H.M. (2016), "Structural performance of ribbed ferrocement plates reinforced with composite materials", *Struct. Eng. Mech.*, **60**(4), 567-594.
Singh, G. (2006), "Finite element analysis of reinforced concrete shear walls", M.Sc. Thesis, Deemed University, India.
Singh, V., Bansal, P.P. and Kumar, M. (2015), "Experimental studies on strength and ductility of ferrocement jacketed RC beam-column joints", *Int. J. Civil Struct. Eng.*, **5**(3), 199-205.
Sirimontree, S., Witchayangkoon, B. and Lertpocasombut, K. (2015), "Strengthening of reinforced concrete column via ferrocement jacketing", *Am. Tran. Eng. Appl. Sci.*, **4**(1), 39-47.

CC

Nomenclatures

V_{rL} = volume fraction in ferrocement element
N = number of layers of mesh
n = number of bars in one layer in the cross section diameter of mesh wire
d_w = diameter of mesh wire
t = thickness of ferrocement layer for calculating the volume fraction in the layer
= thickness of the web for calculating the volume fraction in the web
B = width of the specimen
W_r = unit weight of reinforcing mesh
γ_r = density of reinforcing material
E_c = modulus of elasticity of concrete
F_{cu} = concrete characteristic compressive strength of concrete
ε = concrete strain
ε_o = concrete strain at compressive strength
P_{FC} = 1st crack load
P_{ser} = serviceability load
P_{ult} = ultimate load